The Astrophysical Journal, 622:L133–L136, 2005 April 1

AB AURIGAE RESOLVED: EVIDENCE FOR SPIRAL STRUCTURE

Stuartt Corder, Josh Eisner, and Anneila Sargent
Division of Physics, Mathematics and Astronomy, Mail Code 105-24, California Institute of Technology, 1200 East California Boulevard, Pasadena, CA 91125; sac@astro.caltech.edu, jae@astro.caltech.edu, afs@astro.caltech.edu
Received 2004 December 23; accepted 2005 February 9; published 2005 March 14

ABSTRACT

We have obtained high angular resolution (~2″) images of the ^{13}CO ($J = 1 \rightarrow 0$) line and 2.7 mm continuum emission and slightly lower resolution images of ^{12}CO ($J = 1 \rightarrow 0$) and C^{18}O ($J = 1 \rightarrow 0$) line emission toward the Herbig Ae star AB Aurigae. We resolve a circumstellar disk of diameter 780 AU (FWHM) with a velocity pattern consistent with a purely rotational disk at inclination 21.°5 and position angle 58.°6. Using Keplerian disk models, we find a central-source dynamical mass of $2.8 \pm 0.1\ M_{\odot}$ and a cutoff radius of 615 AU for the ^{13}CO emission. The inclination, mass, and radius determined from ^{12}CO and C^{18}O observations agree with these values, given optical depth and abundance effects. As a result of the high angular resolution of our observations, we confirm the existence of spiral structure suggested by near-infrared scattered-light images and show that the spiral arms represent density contrasts in the disk.

Subject headings: circumstellar matter — stars: individual (AB Aurigae)

1. INTRODUCTION

Circumstellar disks often surround pre–main-sequence objects of low ($\lesssim 2\ M_{\odot}$) and intermediate (~2–10 $M_{\odot}$) mass, the T Tauri and Herbig Ae/Be stars. Disk sizes are on the order of a few hundred AU, with masses a few tenths of a solar mass or less (see, e.g., Beckwith & Sargent 1996; Natta et al. 2000). These values are similar to the proto–solar system (Weidenschilling 1977), suggesting that they may be the sites of planet formation. Disk temperature and density profiles, key properties to understanding how planets might emerge, have been inferred from spatially unresolved observations that rely on spectral energy distributions and require assumptions about disk morphology (e.g., Kenyon & Hartmann 1987; Dullemond et al. 2001). However, higher angular and spectral resolution measurements of the gas and dust in disks are critical to quantifying the profiles directly and providing a context in which to interpret unresolved observations. Spatially and kinematically resolved images enable measurement of stellar mass, disk mass, radius, inclination (i), position angle (P.A.), and substructure (e.g., Koerner et al. 1993; Dutrey et al. 1998; Simon et al. 2000). Such observations of multiple spectral lines in DM Tauri have allowed the exploration of vertical and radial disk structure (Dartois et al. 2003).

The Herbig Ae star AB Aurigae, at 144 pc (ESA 1997), has been studied by numerous authors at optical, IR, and radio wavelengths. Most recently, Semenov et al. (2005, hereafter S05) based a detailed analysis on millimeter observations at 5″–12″ resolution. While this angular resolution is insufficient to determine a stellar mass, their model fits lead to a disk radius of 400 ± 200 AU, $i = 17^{+6}_{-3}$ deg, and P.A. $= 80° \pm 30°$. This inclination agrees well with estimates of $i \lesssim 20°$–$30°$ from near-IR interferometry and scattered light (Millan-Gabet et al. 2001; Eisner et al. 2003, 2004; Grady et al. 1999; Fukagawa et al. 2004, hereafter F04). Earlier millimeter interferometry and recent mid-IR observations at angular resolution ~0.″5 suggest $i \sim 45°$–$70°$ (Marsh et al. 1995; Mannings & Sargent 1997, hereafter MS97; Liu et al. 2005).

High-resolution interferometric images of circumstellar gas can determine the inclination definitively. It is likely that early studies of the AB Aur disk at moderate angular resolution were affected by spiral structure in the disk's surface (F04) or large-scale (~1000 AU) envelope emission (e.g., S05). Here we present high-resolution (2.″2) 2.7 mm continuum and ^{13}CO (1–0) line images and slightly lower resolution maps of the ^{12}CO (1–0) and C^{18}O (1–0) emission from AB Aur. In addition to constraining the disk properties and central mass, these enable us to detect and probe the spiral features seen in the images from F04.

2. OBSERVATIONS AND RESULTS

Observations of AB Aur were carried out between January and May of 2004 at the Owens Valley Radio Observatory (OVRO) millimeter-wave array. Six 10.4 m antennas with cryogenically cooled SIS receivers were used in five array configurations with baselines ranging from 15 to 480 m. We configured the correlator to observe the emission lines of ^{13}CO at 110.2 GHz and ^{12}CO at 115.3 GHz in 64 Hanning-smoothed channels of width 125 kHz, and the C^{18}O emission line at 109.8 GHz in 32 channels of 250 kHz width. The ^{12}CO and C^{18}O observations have maximum baselines of 103 and 120 m, respectively. Simultaneously, we obtained 2.7 mm continuum measurements over 7 GHz of bandwidth with OVRO's COBRA correlator (Hawkins et al. 2004). The quasars J0530 +135 and 3C 111 were observed at 20 minute intervals for phase and amplitude calibration. Absolute flux calibration, accurate to 10%, was based on measurements of Uranus and Neptune. Data reduction was carried out with MIR, an IDL-based package developed for the OVRO array by N. Scoville and J. Carpenter. Maps were made using MIRIAD (Sault et al. 1995).

For AB Aur, Figure 1 shows contours of integrated intensity for ^{12}CO (*left*), ^{13}CO (*middle*), and C^{18}O (*right*) emission at resolutions of 4.″25, 3.″25, and 3.″9, respectively, overlaid on intensity-weighted mean velocity maps (*color*). Integrated line fluxes for ^{12}CO, ^{13}CO, and C^{18}O are 22.1, 3.3, and 0.78 Jy km s^{-1} over the velocity ranges 7.67–4.27, 7.51–4.25, and 7.37–4.63 km s^{-1}, respectively. Outside these ranges, no emission was detected above the 3σ level (360, 105, and 72 mJy beam^{-1} for ^{12}CO, ^{13}CO, and C^{18}O, respectively). We combined our ^{13}CO data set with that of MS97 (rereduced using MIR) to provide greater sensitivity and found that the ^{13}CO flux agrees with that of MS97, within the uncertainties. To emphasize global spatial

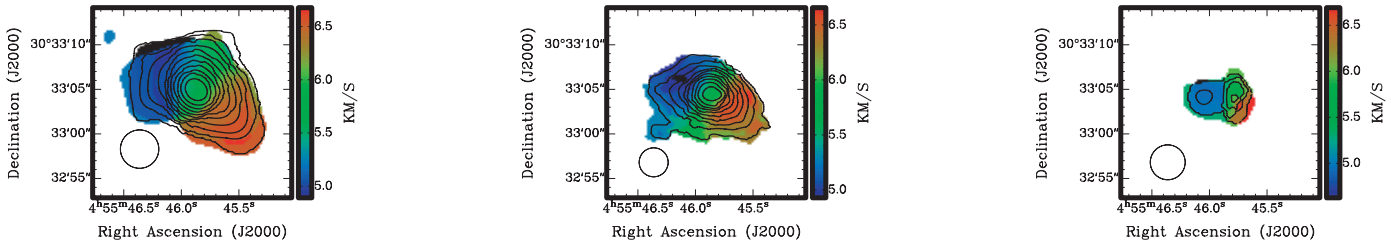

FIG. 1.—OVRO millimeter-array images of the ^{12}CO (*left*), ^{13}CO (*middle*), and C^{18}O (*right*) emission from AB Aur. Intensity-averaged velocity maps (first moment), shown in color, are overlaid with contours of the integrated intensity (zeroth moment). Contours begin at the 3 σ level and are spaced by 3 σ for ^{12}CO and ^{13}CO. For the C^{18}O maps, spacings are 2 σ. The integrated ^{12}CO, ^{13}CO, and C^{18}O maps have 1 σ rms of 145, 36, and 39 mJy km s^{-1}, respectively. Emission was clipped at least at the 4 σ level in the first-moment maps. Circularly restored, naturally weighted equivalent beam sizes are shown in the lower left corners.

and velocity structure, the images were restored with circular beams equal in area to the naturally weighted beams. It is immediately evident that the ^{12}CO and ^{13}CO emission is resolved and the velocity varies smoothly across the maps. Because of lower sensitivity and poorer velocity resolution, the C^{18}O image is barely resolved and the velocity pattern is sufficiently distorted to make analysis difficult.

In the left panel of Figure 2, contours of 2.7 mm continuum emission at resolution 2.″2 are overlaid on a color image of ^{13}CO integrated intensity for AB Aur. Line and continuum emission peaks are spatially coincident to within 0.″3. The optically thin nature of the 2.7 mm emission results in a direct relationship of disk mass to flux, $M_d = 100[F_\nu d^2/\kappa_\nu B_\nu(T)]$. Following MS97, we calculate the disk mass using this expression and the 11.5 mJy flux at 2.7 mm, assuming a gas-to-dust mass ratio of 100 and $\kappa_\nu = 0.009$ cm^2 g^{-1} at 2.7 mm. Adopting a temperature of 40 K, we derive $M_d = 0.009\ M_\odot$ with a factor-of-a-few uncertainty. S05 obtained a similar value, $M_d = 0.013\ M_\odot$, with a factor of 7 uncertainty. The middle panel of Figure 2 displays our 2.7 mm continuum contours overlaid on the near-IR scattered-light image of F04, based on which they suggest spiral structure. While the scattered-light images trace small amounts of material, our 2.7 mm image demonstrates that the spiral features are massive and represent density contrasts, as the 2.7 mm flux directly traces the mass. The three most intense scattered-light features are detected at least at the 3 σ level of significance in 2.7 mm continuum, while the strong northern and southeastern scattered-light arms are at better than the 5 σ level. These northern and southeastern features are more obvious in the right panel of Figure 2. There, the symmetric central core of the continuum image, containing more than 75% of the total flux, has been subtracted to enhance the outer regions. Given the uncertainties in the symmetric source fit, the resulting northeastern and southeastern asymmetry residuals provide 5%–11% and 7%–14% of the total emission, respectively; residual peak locations are uncertain by less than 0.″4, and emission peaks are at least at the 3 σ level.

The smooth velocity gradient in the middle panel of Figure 1 suggests that material is bound to the star and executes Keplerian orbits, a hypothesis supported by S05. The top panels of Figure 3 display the morphology of the ^{13}CO emission in velocity intervals of width 0.34 km s^{-1}. The resolution of these robustly weighted maps, 2.″2 × 1.″8, is almost a factor of 3 better than achieved by MS97 and S05, as is the signal-to-noise ratio. The continuum resolution and signal-to-noise ratio are similarly improved. Robust weighting allows us to emphasize small-scale features in individual velocity bins, as opposed to global characteristics. Enhanced resolution and sensitivity enable a detailed comparison of the line emission at different velocities with that expected from models. The model consists of a flat, Keplerian disk with a single-component power-law emission profile and an outer radius cutoff. The emission profile was fitted empirically, and the emission was binned by line-of-sight velocity and convolved with the 2.″2 × 1.″8 beam. The observed emission was subtracted from the model, and the goodness of fit was measured with a difference-squared merit function. Our best-fit model and 2 σ clipped residuals are presented in the middle and bottom of Figure 3. Our interpretation relies entirely on the ^{13}CO fit. Given the poorer angular and spectral resolution of the ^{12}CO and C^{18}O observations, model fits for those lines were used as consistency checks only. The first three rows of Table 1 list the best-fit parameters for each spectral line.

The best-fit dynamical mass for the ^{13}CO data is 2.8 ± 0.1 $M_\odot$. The disk radius, inclination, and P.A. are 615^{+8}_{-2} AU, $21.^\circ5^{+0.4}_{-0.3}$, and 58.°6 ± 0.°5, respectively. The emission profile has the form $S = 48.4(r/100)^{-1.28}$ mJy inside a radius of 615 AU. Results for the ^{12}CO and C^{18}O are reasonably consistent. We discuss any large discrepancies below. Estimates using other methods to obtain *i*, P.A., and disk radius are shown in the lower portion of Table 1. The uncertainties quoted throughout this work are purely statistical estimates, do not include possible errors in the distance, and are 3 σ for our model fits and 1 σ for other methods. If the velocity pattern is not Keplerian, the errors on all disk parameters except radius could be substantially larger. Disk radius is more correlated with the assumed emission profile.

3. DISCUSSION

Our resolved images of the gas and dust emission from AB Aur enable us to go beyond earlier millimeter observations at lower resolution and determine a central mass of 2.8 ± 0.1 $M_\odot$. This dynamical mass is only a little higher than the 2.4 ± 0.2 $M_\odot$ obtained from photometry and pre–main-sequence track fitting (van den Ancker et al. 1998). Our dynamical model results in several local χ^2 minima, but these are significantly, statistically deviant ($\geq$20 σ) from the global minimum value. Our best-fit values of *i*, P.A., and disk radius (see Table 1) are more accurate than those derived by S05 from lower resolution data and more complex models, and well within their uncertainties.

Large-scale envelope emission, present for $r > 600$ AU (S05), may contaminate more optically thick CO emission. The best-fit ^{12}CO emission profile described in Table 1 indicates structure extending to beyond 1000 AU, and flux ratios of CO isotopomers show that ^{12}CO is optically thick. Given this, the high reduced χ^2 value (~7) for our ^{12}CO model fit is not surprising and demonstrates that a pure-disk model does not fit

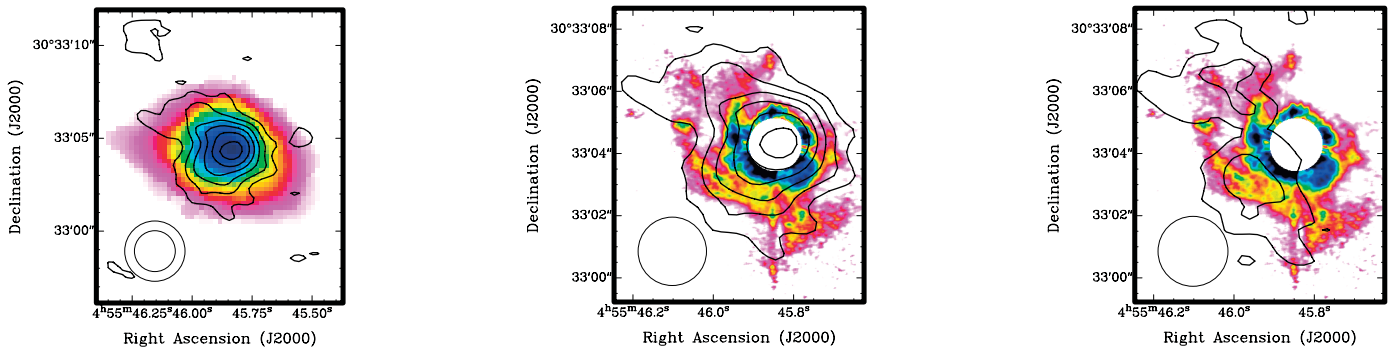

FIG. 2.—*Left*: The 2.7 mm continuum emission for AB Aur (*contours*) overlaid on the ^{13}CO integrated intensity image (*color*). The lower left portion of the map shows the continuum beam size. The ^{13}CO beam surrounds the continuum beam at lower left. Visible ^{13}CO emission begins at the 3 σ level, while the continuum contours begin at 3 σ and increase as 2 σ, where 1 σ is 0.36 mJy beam^{-1}. *Middle*: The same contours of this continuum emission on the scattered-light image from F04. *Right*: Contours of the continuum image with a best-fit Gaussian source subtracted. Contours for this panel begin at 3 σ and increase as 1 σ.

the ^{12}CO emission. The largest deviation of ^{13}CO from the model ($\sim$4.5 σ) occurs in the second velocity bin (see Fig. 3). The deviation is hardly significant and could be due to a number of factors, including local density enhancement, a flared disk surface, etc. A detailed discussion of these is beyond the scope of this work, but there may be some evidence of disk flaring in the top panel of Figure 3, where the southern lobe of emission in bins 4 through 7 splits into two pieces. Given that the ^{13}CO observations fit the pure-disk model much better than ^{12}CO and there is known contamination in the ^{12}CO emission, discrepancies between disk properties derived from ^{12}CO and ^{13}CO can be wholly attributed to this effect, increasing our confidence in the ^{13}CO values.

The model fits to mass and i based on ^{13}CO and C^{18}O emission are consistent within the errors, and the difference in radii is not unexpected given the relatively low abundance of C^{18}O. Our P.A. determinations are consistent with most published values. The inclinations in the first two rows of Table 1 are consistent with near-IR interferometric results (Millan-Gabet et al. 2001; Eisner et al. 2003, 2004) for the inner 1 AU of the disk, and with outer disk values from S05. We checked our model values by calculating i using only the separation of the extreme-velocity emission and, as Table 1 shows, again find good agreement. However, i-values determined from axis ratios in the visibility plane are systematically higher than those from velocity-based methods. Recent determinations of $i = 45°$–$65°$ and P.A. $= 30° \pm 15°$ by Liu et al. (2005), from mid-IR adaptive optics observations with nulling interferometry, agree less well with our model-derived values, and their inclination is much closer to the larger, axis-ratio–determined values of Table 1. We believe that discrepancies between the values of i and P.A. derived by different methods are probably due to assumptions about AB Aur's symmetry.

S05 and F04 demonstrate that the assumption of symmetry is invalid, as do our millimeter observations. The spiral structure, initially suggested by F04 and demonstrated to be a density contrast through this work (see Fig. 2), is a major source of asymmetry. If spiral structure is present and streaming motions along the arms are significant, the gas distribution could be tightened along the arm, resulting in foreshortening perpendicular to that direction. Whether inclination increases or decreases depends on source geometry. In either case, the P.A. will be biased toward the direction of the long axis of the spiral arm. Spiral structure could also affect the i and P.A. determined from velocity structure, depending on the strength of the features and the optical thickness of the line; optically thinner emission features would experience greater influence from such local density enhancements. Sub-Keplerian rotation will generally result in larger inclinations for velocity-determined methods with fixed mass, but a simple sub-Keplerian disk aided by gas pressure is probably too simplistic an assumption if streaming motions are altering the bulk of the gas motion along the arms.

Our observations show two effects that could be due to the

TABLE 1
BEST-FIT MODEL PARAMETERS

Method	Line	Mass ($M_\odot$)	Radius (AU)	Inclination (deg)	Position Angle (deg)
Line model	^{13}CO	2.8 ± 0.1	615^{+8}_{-3}	$21.5^{+0.4}_{-0.3}$	58.6 ± 0.5
	C^{18}O	$2.77^{+0.09}_{-0.15}$	497^{+10}_{-3}	$21.4^{+0.7}_{-0.3}$	75 ± 2
	^{12}CO	$3.25^{+0.13}_{-0.14}$	1060 ± 10	$32.5^{+0.4}_{-0.5}$	61 ± 3
Extreme velocity	^{13}CO	2.8	...	24 ± 4	69 ± 8
	C^{18}O	2.8	...	17 ± 6	73 ± 21
	^{12}CO	2.8	...	26 ± 9	66 ± 25
(u, v)-plane	^{13}CO	...	390 ± 15	33 ± 5	85 ± 10
	^{12}CO	...	500 ± 13	41 ± 3	26 ± 4
	Dust	...	170 ± 17	44 ± 12	79 ± 19

NOTES.—"Dust" is the 2.7 mm continuum emission. Error bars are 1 σ for all but the line model, where errors are 3 σ. Radii are half-width at half-maximum values except for the line models, where they represent outer edges of the disk. The emission profile for the line model was of the form $S = S_0[r/(100\ \mathrm{AU})]^{-k}$ mJy for $r \le R_{\mathrm{out}}$. Values (S_0, k) are ($48.4^{+1.3}_{-0.8}$, 1.28 ± 0.04), ($13.4^{+1.2}_{-1.9}$, $1.30^{+0.06}_{-0.08}$), and (150 ± 2, 1.1 ± 0.1) for ^{13}CO, C^{18}O, and ^{12}CO, respectively.

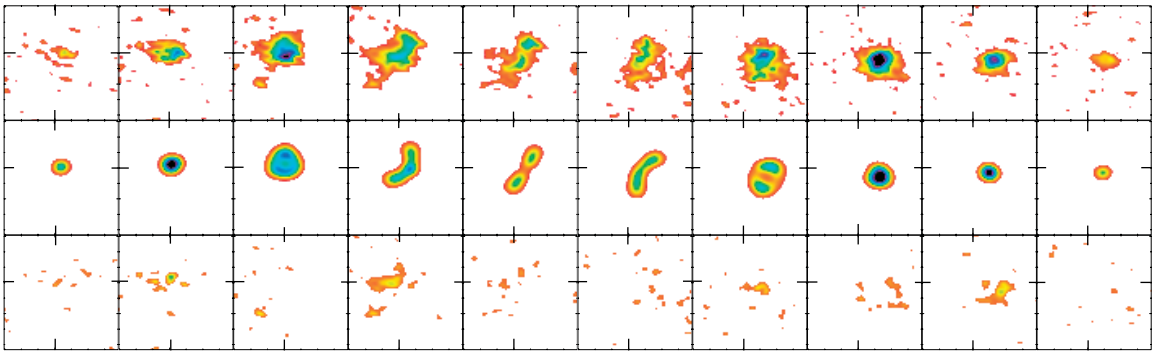

FIG. 3.—*Top*, ^{13}CO observations with 2.″2 × 1.″8 resolution and 1 σ rms noise of 35 mJy beam^{-1}; *middle*, best-fit Keplerian model, with mass 2.8 $M_{\odot}$, i = 21.°5, and P.A. = 58.°6; *bottom*, residuals of the data and model clipped at 2 σ. Red, yellow, green, blue, and dark blue emission represent approximately 2, 3.5, 5.0, 6.5 and 8.5 σ above the noise. The leftmost images have velocity 4.27 km s^{-1}, and the image velocity width is 0.34 km s^{-1}. Large tick marks define the position α = 04^{h}55^{m}46^{s}, δ = 30°33′05″ (J2000). Right ascension ranges from 46.^{s}58 to 45.^{s}23 from left to right, and the declination extends from 32′54.″8 to 33′12.″3 from bottom to top.

influence of spiral structure: (1) The model fit to the optically thin C^{18}O line leads to a significantly greater P.A. than does the ^{13}CO fit. The direction of change of the position angle is along the strong southeastern arm, as would be expected if local streaming velocities were playing a role. (2) In the left panel of Figure 2, the ^{13}CO emission spreads well beyond the boundaries of the continuum emission in the northeast and southwest but has a similar extent in the southeast. If spiral structure is changing gas morphology, it would cause *larger* spatially determined inclinations and P.A.'s, thereby explaining the higher inclinations estimated from axis ratios. We conclude that the range of published values of inclination and P.A. can be explained by the presence of substructure. The values derived from our kinematic models may be influenced by this substructure, but we do not expect the effects to be great.

The wealth of observations of AB Aur at different wavelengths and at different spatial and spectral resolutions enable analysis of this complicated circumstellar disk from the inner 1 AU (e.g., Eisner et al. 2004) to the outer envelope beyond 1000 AU (e.g., Semenov et al. 2005). Our detailed observations give an accurate dynamical mass and resolve issues about i and P.A., indicating that apparent inconsistencies are due to asymmetry. Our high-resolution images in 2.7 mm continuum and ^{13}CO and C^{18}O gas emission show evidence of spiral structure. Such structure has important implications for planet formation. If it is due to instability and persists long enough or is sufficiently strong, then local collapse can occur, quickly forming large planets (Boss 2002; Pickett et al. 2003; references therein). Alternatively, if the instability dissipates or the structure is due to existing planets (Bate et al. 2003), the increase in local density may increase the cross section for collisions of planetesimals and speed up the core accretion process (Rice et al. 2004).

Research with the OVRO array is funded in part by NSF grant AST 99-81546. S. C. is supported by an NSF Graduate Research Fellowship, and J. E. by a Michelson Fellowship. We thank M. Fukagawa for providing her scattered-light image of AB Aur, J. Carpenter for interest and advice, and the referee, A. Natta, for constructive comments.

REFERENCES

Bate, M. R., Lubow, S. H., Ogilvie, G. I., & Miller, K. A. 2003, MNRAS, 341, 213
Beckwith, S. V. W., & Sargent, A. I. 1996, Nature, 383, 139
Boss, A. P. 2002, ApJ, 576, 462
Dartois, E., Dutrey, A., & Guilloteau, S. 2003, A&A, 399, 773
Dullemond, C. P., Dominik, C., & Natta, A. 2001, ApJ, 560, 957
Dutrey, A., Guilloteau, S., Prato, L., Duvert, G., Schuster, K., & Ménard, F. 1998, A&A, 338, L63
Eisner, J. A., Lane, B. F., Akeson, R. L., Hillenbrand, L. A., & Sargent, A. I. 2003, ApJ, 588, 360
Eisner, J. A., Lane, B. F., Hillenbrand, L. A., Akeson, R. L., & Sargent, A. I. 2004, ApJ, 613, 1049
ESA. 1997, The *Hipparcos* and Tycho Catalogues (ESA SP-1200) (Noordwijk: ESA)
Fukagawa, M., et al. 2004, ApJ, 605, L53 (F04)
Grady, C. A., Woodgate, B., Bruhweiler, F. C., Boggess, A., Plait, P., Lindler, D. J., Clampin, M., & Kalas, P. 1999, ApJ, 523, L151
Hawkins, D. W., Woody, D. P., Wiitala, B., Fredsti, J., & Rauch, K. P. 2004, Proc. SPIE, 5498, 567
Kenyon, S. J., & Hartmann, L. 1987, ApJ, 323, 714
Koerner, D. W., Sargent, A. I., & Beckwith, S. V. W. 1993, Icarus, 106, 2
Liu, W. M., Hinz, P. M., Hoffmann, W. F., Brusa, G., Miller, G., & Kenworthy, M. A. 2005, ApJ, 618, L133
Mannings, V., & Sargent, A. I. 1997, ApJ, 490, 792 (MS97)
Marsh, K. A., Van Cleve, J. E., Mahoney, M. J., Hayward, T. L., & Houck, J. R. 1995, ApJ, 451, 777
Millan-Gabet, R., Schloerb, F. P., & Traub, W. A. 2001, ApJ, 546, 358
Natta, A., Grinin, V. P., & Mannings, V. 2000, in Protostars and Planets IV, ed. V. Mannings, A. P. Boss, & S. S. Russell (Tucson: Univ. Arizona Press), 559
Pickett, B. K., Mejía, A. C., Durisen, R. H., Cassen, P. M., Berry, D. K., & Link, R. P. 2003, ApJ, 590, 1060
Rice, W. K. M., Lodato, G., Pringle, J. E., Armitage, P. J., & Bonnell, I. A. 2004, MNRAS, 355, 543
Sault, R. J., Teuben, P. J., & Wright, M. C. H. 1995, in ASP Conf. Ser. 77, Astronomical Data Analysis Software and Systems IV, ed. R. A. Shaw, H. E. Payne, & J. J. E. Hayes (San Francisco: ASP), 433
Semenov, D., Pavlyuchenkov, Ya., Schreyer, K., Henning, T., Dullemond, K., & Bacmann, A. 2005, ApJ, 621, 853 (S05)
Simon, M., Dutrey, A., & Guilloteau, S. 2000, ApJ, 545, 1034
van den Ancker, M. E., Winter, D., & Tjin A Djie, H. R. E. 1998, A&A, 330, 145
Weidenschilling, S. J. 1977, Ap&SS, 51, 153